

REPORTS

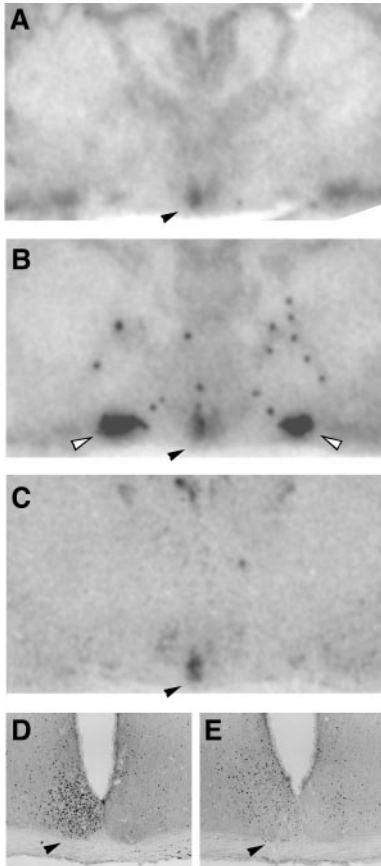


Fig. 3. SCN AVP and *c-fos* gene expression in the behaviorally split hamster. Coronal brain sections through the SCN were processed for in situ hybridization. SCN AVP mRNA levels were relatively high [black arrowhead in (B)] on the side of the SCN ipsilateral to high *Per1* expression [arrowhead in (A)]; AVP levels in the supraoptic nuclei were symmetrical [open arrowheads in (B)]; black dots in the autoradiograph are small clusters of magnocellular AVP perikarya]. SCN *c-fos* mRNA levels were relatively high [arrowhead in (C)] on the same side as *Per1* and AVP, and immunohistochemistry for the *c-Fos* protein showed a unilateral rostral [arrowhead in (D)] and dorsal [arrowhead in (E)] distribution. Scale bars: 1.1 mm, (A) to (C); 400 μ m, (D) and (E).

and right-sided circadian oscillators. This is a unique neural state, a “split” brain without surgical bisection. Because AVP is a neurotransmitter controlled by the SCN clock, and because AVP and other SCN efferents project ipsilaterally to their targets (37), other bilaterally represented brain regions outside the SCN may also be running on antipodal time.

References and Notes

1. D. C. Klein, R. Y. Moore, S. M. Reppert, Eds., *Suprachiasmatic Nucleus: The Mind's Clock* (Oxford Univ. Press, New York, 1991).
2. D. K. Welsh, D. E. Logothetis, M. Meister, S. M. Reppert, *Neuron* **14**, 697 (1995).
3. D. P. King, J. S. Takahashi, *Annu. Rev. Neurosci.* **23**, 713 (2000).
4. C. S. Pittendrigh, S. Daan, *J. Comp. Physiol. A* **106**, 333 (1976).

5. C. A. Shibuya, R. B. Melnyk, N. Mrosovsky, *Naturwissenschaften* **67**, 45 (1980).
6. G. E. Pickard, R. Kahn, R. Silver, *Physiol. Behav.* **32**, 763 (1984).
7. J. M. Swann, F. W. Turek, *Science* **228**, 898 (1985).
8. P. Zlomanczuk, R. R. Margraf, G. R. Lynch, *Brain Res.* **559**, 94 (1991).
9. S. Daan, C. Berde, *J. Theor. Biol.* **70**, 297 (1978).
10. J. G. Lees, J. D. Hallonquist, N. Mrosovsky, *J. Comp. Physiol. A* **153**, 123 (1983).
11. Z. Boulos, L. P. Morin, *J. Biol. Rhythms* **1**, 1 (1986).
12. J. H. Meijer, S. Daan, G. J. F. Overkamp, P. M. Hermann, *J. Biol. Rhythms* **5**, 1 (1990).
13. G. E. Pickard, F. W. Turek, *Science* **215**, 1119 (1982).
14. M. E. Harrington, G. A. Eskes, P. Dickson, B. Rusak, *Brain Res. Bull.* **24**, 593 (1990).
15. M. Akiyama et al., *J. Neurosci.* **19**, 1115 (1999).
16. B. Zheng et al., *Nature* **400**, 169 (1999).
17. Linearized recombinant plasmids were used as templates for the generation of antisense cRNA probes: hamster *Per1* [783–base pair (bp) cDNA insert in Bluescript II SK+], hamster *Per2* (791-bp insert in pGEM-T Easy), hamster *Per3* (819-bp insert in pGEM-T Easy), hamster *Bmal1* (2.4-kb insert in pVP16), rat *c-fos* (2.3-kb insert in pSP65), and rat AVP (241-bp insert in pGEM3). Probes were transcribed in the presence of [³⁵S]uridine triphosphate with the appropriate RNA polymerases with the MaxiScript kit (Ambion). Hamsters were decapitated, brains were rapidly removed and frozen, and in situ hybridization was performed on 15- μ m-thick coronal sections as previously described (38).
18. U. Albrecht, Z. S. Sun, G. Eichele, C. C. Lee, *Cell* **91**, 1055 (1997).
19. T. Takumi et al., *EMBO J.* **17**, 4753 (1998).
20. E. S. Maywood, N. Mrosovsky, M. D. Field, M. H. Hastings, *Proc. Natl. Acad. Sci. U.S.A.* **96**, 15211 (1999).
21. S. Honma et al., *Biochem. Biophys. Res. Commun.* **250**, 83 (1998).
22. L. P. Shearman et al., *Science* **288**, 1013 (2000).
23. X. Jin et al., *Cell* **96**, 57 (1999).
24. S. M. Reppert, W. J. Schwartz, G. R. Uhl, *Trends Neurosci.* **10**, 76 (1987).
25. I. Chambille, S. Doyle, J. Servièrre, *Brain Res.* **612**, 138 (1993).
26. M. E. Guido, D. Goguen, L. De Guido, H. A. Robertson, B. Rusak, *Neuroscience* **90**, 555 (1999).
27. Hamsters were deeply anesthetized with pentobarbital (20 mg per 100 g of body weight, intraperitoneal) and perfused with 25 ml of heparinized 0.01 M phosphate-buffered saline followed by 100 ml of cold 4% paraformaldehyde in 0.1 M phosphate buffer. Brains were postfixed overnight at 4°C, and 40- μ m-thick sections were incubated with antiserum to *c-Fos*₃₋₁₇ (1:10,000; SC52; Santa Cruz Biotechnology) for 48 hours at 4°C and processed for immunohistochemistry as described (38).
28. D. J. Hudson, M. E. Lickey, *Brain Res.* **183**, 481 (1980).
29. W. K. Koehler, G. Fleissner, *Nature* **274**, 708 (1978).
30. T. L. Page, *J. Comp. Physiol. A* **124**, 225 (1978).
31. G. Wiedenmann, *J. Comp. Physiol. A* **150**, 51 (1983).
32. J. D. Palmer, *Bioessays* **22**, 32 (2000).
33. A. Sumová, H. Illnerová, *Am. J. Physiol.* **274**, R857 (1998).
34. A. Jagota, H. O. de la Iglesia, W. J. Schwartz, *Nature Neurosci.* **3**, 372 (2000).
35. F. C. Davis, R. A. Gorski, *J. Comp. Physiol. A* **154**, 221 (1984).
36. F. C. Davis, N. Viswanathan, *J. Biol. Rhythms* **11**, 291 (1996).
37. A. Kalsbeek, R. Teclemariam-Mesbah, P. Pévet, *J. Comp. Neurol.* **332**, 293 (1993).
38. W. J. Schwartz et al., *Neuroscience* **98**, 535 (2000).
39. We thank T. Curran, H. Okamura, S. Shibata, T. Sherman, and C. Weitz for gifts of recombinant plasmids. Supported by R01 NS24542 (to W.J.S.).

27 June 2000; accepted 13 September 2000

Integration of Multiple Signals Through Cooperative Regulation of the N-WASP–Arp2/3 Complex

Kenneth E. Prehoda,^{1,2} Jessica A. Scott,^{1,2} R. Dyché Mullins,¹ Wendell A. Lim^{1,2*}

The protein N-WASP [a homolog to the Wiskott-Aldrich syndrome protein (WASP)] regulates actin polymerization by stimulating the actin-nucleating activity of the actin-related protein 2/3 (Arp2/3) complex. N-WASP is tightly regulated by multiple signals: Only costimulation by Cdc42 and phosphatidylinositol (4,5)-bisphosphate (PIP₂) yields potent polymerization. We found that regulation requires N-WASP's constitutively active output domain (VCA) and two regulatory domains: a Cdc42-binding domain and a previously undescribed PIP₂-binding domain. In the absence of stimuli, the regulatory modules together hold the VCA–Arp2/3 complex in an inactive “closed” conformation. In this state, both the Cdc42- and PIP₂-binding sites are masked. Binding of either input destabilizes the closed state and enhances binding of the other input. This cooperative activation mechanism shows how combinations of simple binding domains can be used to integrate and amplify coincident signals.

Many cellular processes are controlled by networks of interacting signaling pathways (1, 2). For example, during directed cell motility, multiple pathways converge to precisely target actin polymerization to the cell's

leading edge. Little is known, however, about the molecular mechanisms by which the relevant signaling proteins integrate these multiple inputs to yield a coordinated response.

WASP and its homolog N-WASP link

multiple signaling pathways to actin assembly (3–5). N-WASP interacts with the Arp2/3 complex and activates its ability to nucleate actin filaments (5, 6). Activation only occurs, however, when N-WASP is stimulated by the proper set of upstream signals. The two best characterized inputs are the rho family guanosine triphosphatase (GTPase) Cdc42 and phosphatidylinositol 4,5-bisphosphate (PIP₂), both of which are regulated by upstream pathways critical for motility (1, 7, 8). Individually, Cdc42 and PIP₂ are weak activators of N-WASP. Together, however, the inputs act synergistically: costimulation with low concentrations of both yields potent activation (5). Thus, N-WASP acts as a signal integration device that can precisely target actin polymerization to sites on the membrane at which both PIP₂ and activated Cdc42 are present.

Several domains within N-WASP have been implicated in this signal processing behavior (Fig. 1A). Output is controlled by a COOH-terminal domain that directly interacts with and activates the Arp2/3 complex

(5). This domain is referred to as the VCA domain (also called WWA) because it has a verprolin homology motif (V), a cofilin homology motif (C), and an acidic motif (A). The acidic motif binds Arp2/3, whereas the verprolin motif binds actin monomers, probably delivering them to Arp2/3 (5, 6). The isolated VCA domain is constitutively active; however, this activity is suppressed in full-length N-WASP, indicating that NH₂-terminal regions play a regulatory role (5). One key regulatory domain is the GTPase-binding domain (GBD), which forms an intramolecular interaction with the cofilin homology motif (Fig. 1A) (9, 10). Because activated Cdc42 can disrupt the intramolecular interaction by binding the GBD, a simple model for N-WASP regulation has been proposed: the intramolecular interaction between the GBD and the cofilin motif blocks binding of Arp2/3 to the VCA domain, and Cdc42 relieves this autoinhibitory interaction (3, 5, 9). There are several problems with this model. First, the GBD has never experimentally been shown to block Arp2/3 binding or to suffice as a functional repressor of the VCA domain. Second, this simple autoinhibition model fails to explain how PIP₂ is detected as an input, and how its effects are synergistically integrated with those of Cdc42.

To elucidate the mechanism of N-WASP regulation and signal integration, we identified

the minimal domains required to repress the VCA domain, mapped their interactions, and determined how they communicate. We found that two adjacent regulatory domains, the GBD and a novel PIP₂-binding motif, are necessary and sufficient for proper repression and regulation of N-WASP. In the absence of stimuli, the two regulatory motifs together lock the VCA-Arp2/3 complex in an inactive “closed” conformation. The mechanism of repression allows for highly cooperative activation: Cdc42 and PIP₂ disrupt the closed state in a thermodynamically coupled fashion, providing the basis for potent signal integration by N-WASP.

VCA domain activity was potently repressed (inhibition constant $K_i = \sim 1 \mu\text{M}$) by a minimal fragment containing both the GBD and an adjacent, highly basic motif in an *in vitro* actin polymerization assay (Fig. 1B). We refer to this composite domain as the “control region.” The basic motif is only ~20 residues in length and contains nine lysine residues (11). In contrast, a second fragment consisting solely of the GBD, although able to interact strongly with the VCA domain, had virtually no inhibitory effect (Fig. 1B), even at concentrations (100 μM) well above saturation (12). The GBD failed to inhibit even when covalently tethered (*cis*) to the VCA domain (13). A third fragment that contains the basic motif and only half of the GBD was also unable to repress (Fig. 1B). These data show that current models for autoinhibition are incorrect: although required, the GBD alone is insufficient to repress VCA activation of the Arp2/3 complex; rather, the composite control region is the minimal repressive element.

Remarkably a “mini-N-WASP” that contains only the control region and the VCA domain attached by a nine-residue linker is also sufficient to recapitulate the hallmark regulatory behavior of N-WASP. Its Arp2/3 stimulatory activity is highly repressed but can be synergistically activated by costimulation with PIP₂ and Cdc42 complexed with guanosine 5'-O-(3'-thiotriphosphate) (Cdc42-GTP γ S) (Fig. 1C) (14).

Contrary to previous models, we found that neither the control region nor GBD blocks binding of Arp2/3 to the VCA domain (Fig. 2A) (15). Instead, the basic motif participates in two previously uncharacterized interactions critical for regulation (Fig. 2, B through D). First, the basic motif is an essential part of a novel Arp2/3 binding site (Fig. 2B). Although this Arp2/3 interaction region appears to be crucial for repression, it is not sufficient, because a fragment that binds Arp2/3 but lacks the intact GBD (residues 178 through 244) also fails to inhibit VCA activity (Fig. 1B). Arp2/3 therefore interacts with two sites within N-WASP: the acidic motif within the VCA domain and the basic motif within the control region. Second, we found that the basic region is also a novel

¹Department of Cellular and Molecular Pharmacology, and ²Department of Biochemistry and Biophysics, University of California, San Francisco, CA 94143–0450, USA.

*To whom correspondence should be addressed. E-mail: wlim@itsa.ucsf.edu

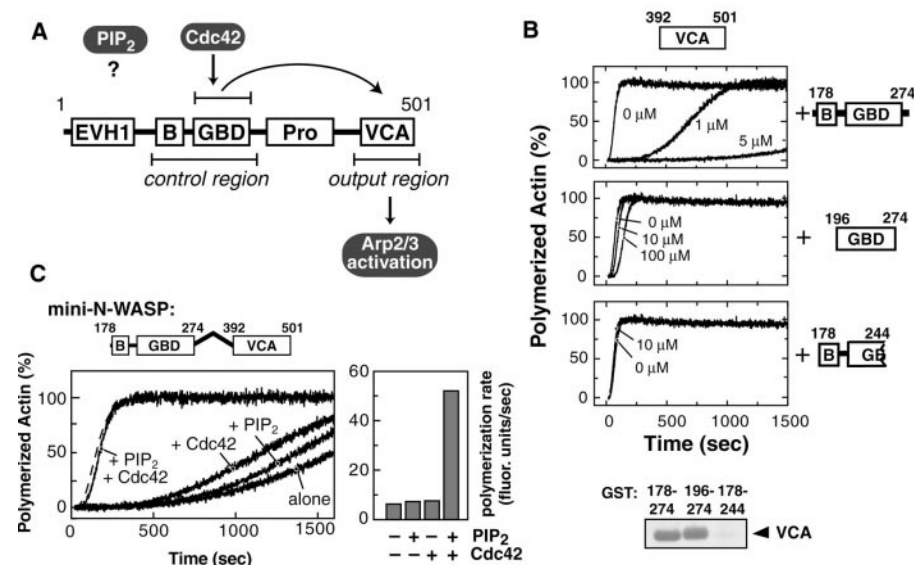


Fig. 1. Both the basic motif and GBD are required for repression and regulation of N-WASP. (A) N-WASP contains the following domains: EVH1 domain, basic motif (B), GBD, proline-rich motif (Pro), and verprolin/cofilin/acidic domain (VCA). Curved arrow indicates intramolecular interaction between GBD and the cofilin motif (within the VCA domain) (9, 10). (B) Repression of VCA-Arp2/3-mediated actin polymerization by control region fragments (25), tested using *in vitro* pyrene actin polymerization assay (26). Assays contain 50 nM VCA, 50 nM Arp2/3, and 2.5 μM actin (2% pyrene actin), along with the indicated concentration of variable fragment. Binding of the VCA domain to these control region fragments fused to GST (27) is shown below. (C) Mini-N-WASP (178–274-GSGSGSGS–392–501) mimics the regulatory behavior of N-WASP (28). Pyrene actin polymerization assays are shown for mini-N-WASP alone and mini-N-WASP plus Cdc42-GTP γ S (0.15 μM), PIP₂ (~0.4 μM in PS:PC:PIP₂ vesicles at 48:48:2), or both (same concentrations as above). Activity of VCA domain alone (dotted line) is shown for comparison. Assays contain 50 nM mini-N-WASP, 50 nM Arp2/3, and 2.5 μM actin. Bar graph shows maximal polymerization rate for each assay.

REPORTS

phospholipid-binding module that specifically recognizes PIP₂ (Fig. 2C). This 20-residue motif is distinct from larger canonical phospholipid-binding domains, such as pleckstrin homology (16) or FYVE finger domains (17).

The interactions of the control region (Fig. 2D) and the requirements for repression (Fig. 1B) support a concerted repression model. Neither the GBD nor the basic motif is intrinsically repressive; rather, each alone is a neutral anchor point that, only when topologically linked to and acting in concert with the other, locks the N-WASP–Arp2/3 complex in an inactive “closed” state (Fig. 2D). These interactions may alter the conformation of Arp2/3 and/or its relationship with the VCA domain, rendering it inactive. This model is supported by the finding that when the GBD and basic modules are added together, but as covalently distinct elements, they fail to repress VCA domain activity (13).

Moreover, these control region subfragments are found to activate mini-N-WASP (Fig. 2E), behavior incompatible with subfragments that are intrinsically repressive (these would repress or be neutral). The behavior is best explained as uncoupling of concerted interactions required for repression (Fig. 2E).

The novel mechanism of N-WASP repression suggests a reciprocal mechanism for activation by both Cdc42 and PIP₂. These inputs bind the GBD and basic motifs, respectively, and thus either could disrupt the “closed” state and release the active VCA–Arp2/3 complex. Activated Cdc42 is known to disrupt the intramolecular GBD–VCA interaction (9, 10). We find that Cdc42 also disrupts the control region–Arp2/3 interaction (Fig. 3A). However, this alone cannot explain synergistic activation by PIP₂ and Cdc42.

Synergistic activation could be explained, however, if PIP₂ and Cdc42 act cooperatively to disrupt the closed state. Therefore, we

tested if binding of the two inputs is thermodynamically coupled. Vesicle-binding studies show that PIP₂ and Cdc42 can bind the control region simultaneously (Fig. 3B), and that in the context of mini-N-WASP, Cdc42 can dramatically enhance PIP₂ binding (Fig. 3C). Moreover, parallel fluorescence binding studies show that PIP₂ can enhance Cdc42 binding to the control region, in the presence of Arp2/3 (Fig. 3D). Thus, cooperative binding of PIP₂ and Cdc42 to N-WASP has been observed.

However, this observed cooperativity discussed above cannot result from direct interaction between Cdc42 and PIP₂, because the two inputs do not bind cooperatively to the isolated control region (Fig. 3, C and D). Instead, cooperativity must result from coordinated competition with other control region (B–GBD) ligands. For example, interaction of the control region with the VCA domain, present in mini-N-WASP, appears to mask both the PIP₂- and

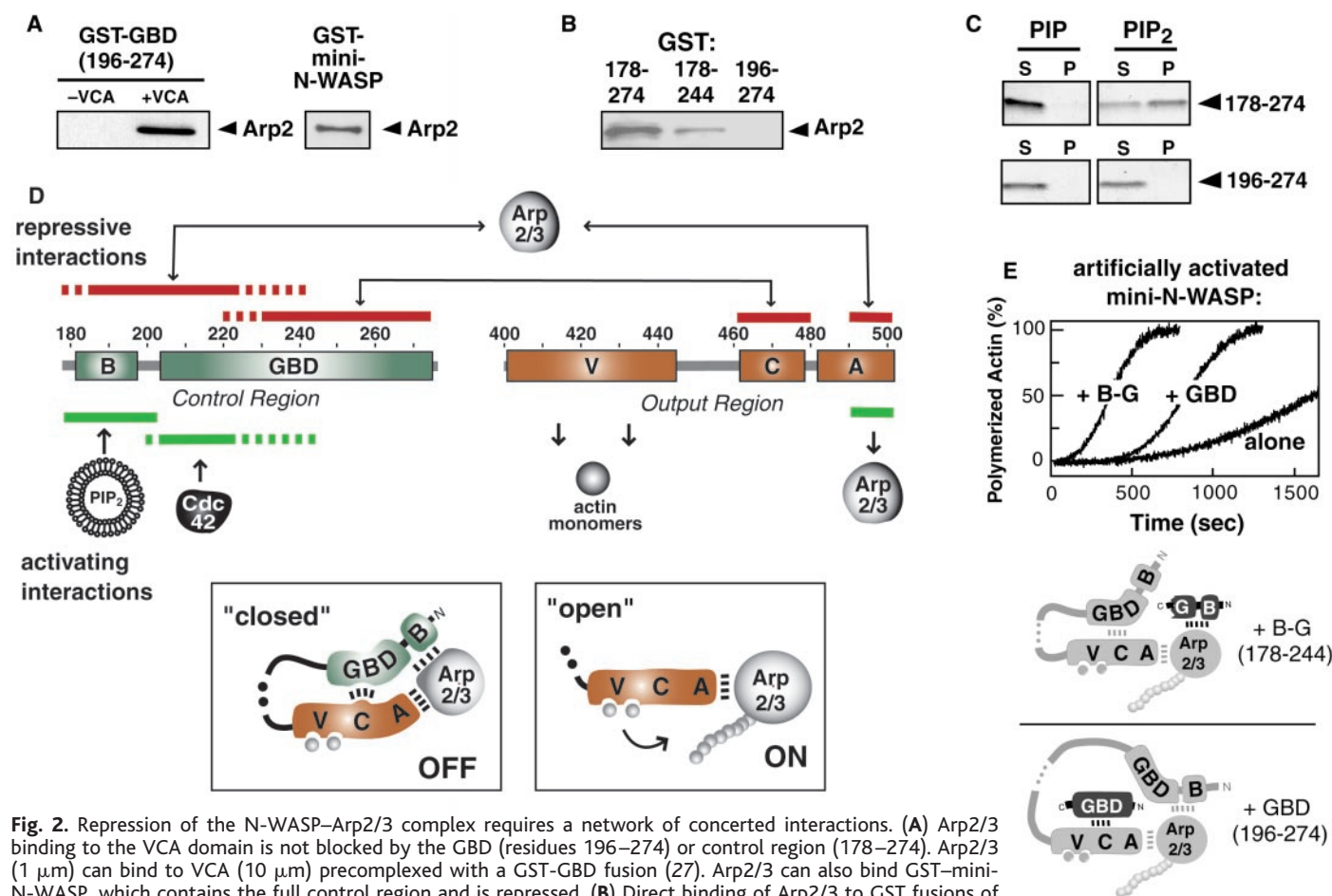


Fig. 2. Repression of the N-WASP–Arp2/3 complex requires a network of concerted interactions. **(A)** Arp2/3 binding to the VCA domain is not blocked by the GBD (residues 196–274) or control region (178–274). Arp2/3 (1 μ M) can bind to VCA (10 μ M) precomplexed with a GST–GBD fusion (27). Arp2/3 can also bind GST–mini-N-WASP, which contains the full control region and is repressed. **(B)** Direct binding of Arp2/3 to GST fusions of control region fragments (27). **(C)** PIP and PIP₂ vesicle spin-down binding assays (29). S indicates supernatant (unbound) and P indicates pellet (bound). Control region (residues 178–274) can selectively bind PIP₂ whereas the GBD alone (residues 196–274) cannot. **(D)** Summary of control region and output region interactions mapped in this study [complete supplementary data is given in Web fig. 1 (30)]. Solid lines are essential regions; dotted lines are important but nonessential regions. Also shown is a cartoon of the repressed, “closed” state of the N-WASP–Arp2/3 complex (31). The interactions in the closed state could repress by inducing a conformational change in Arp2/3 and/or the VCA domain, or a change in the arrangement of the two components. Disruption of these interactions allows conversion to the active, “open” state. **(E)** Artificial disruption of the repressive network leads to activation. Control region subfragments consisting of either the GBD alone, or the basic motif with a truncated GBD (+B-G), activate mini-N-WASP. Actin polymerization assays were performed with 80 nM mini-N-WASP \pm 10 μ M of either subfragment. The postulated mechanism of artificial activation is shown.

REPORTS

Fig. 3. Cdc42 and PIP₂ bind cooperatively to N-WASP when competing against repressive interactions. (A) Cdc42-GTPγS inhibits Arp2/3 binding to a GST-control region fragment (27). (B) PIP₂ vesicle binding assays (29) show that Cdc42-GTPγS and PIP₂ can simultaneously bind the control region (B-GBD). S indicates supernatant (unbound) and P indicates pellet (bound). Cdc42-GTPγS does not bind to PIP₂ vesicles in the absence of the control region (not shown). (C) Cdc42-GTPγS enhances mini-N-WASP binding to PIP₂. In the absence of Cdc42, mini-N-WASP binds poorly to PIP₂, most likely because the GBD-VCA interaction sterically masks the PIP₂-binding site. High-affinity PIP₂ binding is observed if Cdc42 is present, or if the VCA domain is removed. The cooperative effects between Cdc42 and PIP₂ are not observed for binding to the control region alone (B-GBD). (D) PIP₂ enhances apparent affinity of Cdc42 for the control region-Arp2/3 complex. Dissociation constants for the control region interaction with fluorescently tagged Cdc42 (32), either alone (K_d) or with additional factors (K_d^{app}), were measured as described in Web fig. 2 (30). We added 2.5 μM of Arp2/3 or 10 μM of PIP₂ (PC:PS:PIP₂ at ratios of 48:48:2), or both. The presence of Arp2/3 significantly decreases the apparent affinity, as expected, because Arp2/3 competes against Cdc42 for binding to the control region (A). However, addition of PIP₂ with Arp2/3 restores the higher apparent affinity, indicating that PIP₂ and Cdc42 cooperate to compete against Arp2/3 binding. Cooperation is not observed in the absence of Arp2/3.

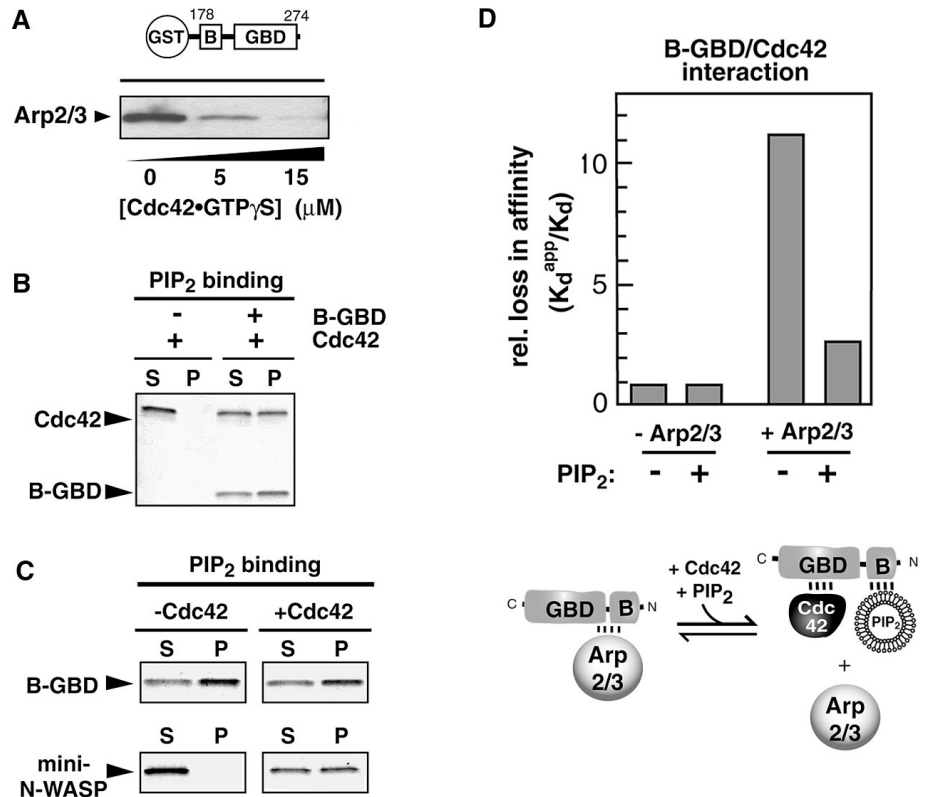
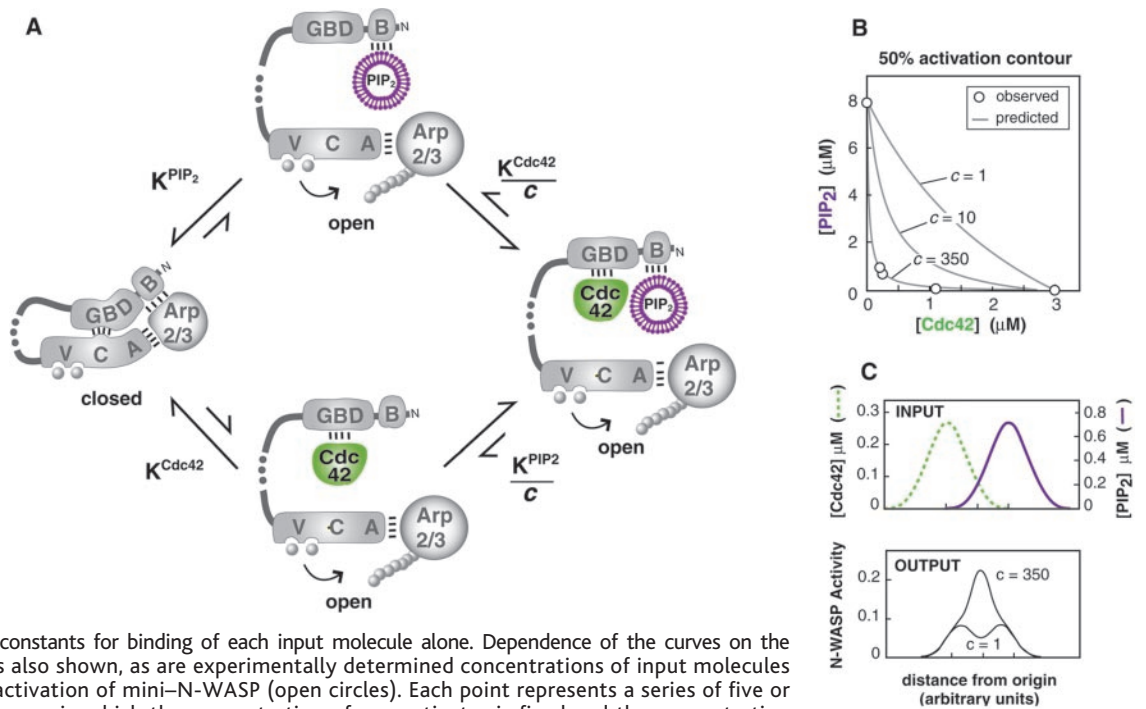


Fig. 4. Highly cooperative activation mechanism of N-WASP allows for potent signal integration. (A) Thermodynamic cycle modeling states of Cdc42 (green) and PIP₂ (purple) binding to mini-N-WASP. Binding of a second input molecule is more favorable, because the energetic cost of disrupting the closed state is paid by binding of the first input molecule. The degree of enhancement in binding is given by the cooperativity factor, c . (B) Theoretical curves indicate the concentration of two input molecules required to achieve 50% activation of a protein switch such as that modeled in (A) (33). Intercepts give the dissociation constants for binding of each input molecule alone. Dependence of the curves on the cooperativity constant, c , is also shown, as are experimentally determined concentrations of input molecules required to achieve 50% activation of mini-N-WASP (open circles). Each point represents a series of five or six actin polymerization assays in which the concentration of one activator is fixed and the concentration of the second activator is varied [Web fig. 3 (30)]. The 50% activation points (K_{act}) are determined based on maximal rates of actin polymerization. Data fit the model with $c \approx 350$. (C) Cooperativity provides a mechanism for signal integration. Top graph shows hypothetical, spatially overlapping concentration gradients of Cdc42-GTP (green) and PIP₂ (purple). The bottom graph shows the calculated response of N-WASP (fraction maximal activity) assuming the model in (A) and a cooperativity of either 1 or 350. With high cooperativity, coincident signals are integrated and amplified.



Cdc42-binding sites (Fig. 3C). Thus, Cdc42 strongly enhances PIP₂ binding in this context. Arp2/3 binding to the control region also ap-

pears to mask both the Cdc42- and PIP₂-binding sites, explaining the cooperative effects of the two inputs in this context (Fig. 3D). In

summary, it is the structure and interactions within the closed state that makes binding of the two inputs highly cooperative.

The activation behavior of N-WASP can thus be modeled, using the thermodynamic cycle shown in Fig. 4A. In the repressed state, a network of interactions holds the N-WASP-Arp2/3 complex in a closed state. Cdc42 and PIP₂ can individually disrupt this network and activate the complex. However, because their binding sites are masked by repressive interactions, binding of either input alone to the closed state is relatively weak. In contrast, if one input molecule is prebound, the closed state is destabilized, and binding of the second molecule is considerably enhanced. The degree to which binding of one ligand enhances binding of the other is determined by the cooperativity factor, *c*. This behavior is analogous to that of any cooperative binding protein, such as hemoglobin (18, 19), although in this case, cooperativity is observed between heterotropic rather than homotropic ligands. Nonetheless, both mechanisms involve increasing stabilization of an open or relaxed state by binding of successive ligands.

This framework reveals that a highly cooperative activation mechanism allows for potent signal integration. A series of simulated contours indicating the concentrations of two activating inputs required to achieve 50% activation is shown in Fig. 4B. If two input ligands are completely independent (*c* = 1), their combined effects are nearly additive and the 50% activation contour will be close to linear. In contrast, if *c* is high, the two ligands will act synergistically. The 50% activation contour will be concave, because when added together, significantly lower concentrations of each ligand are required for activation.

We experimentally measured activation of mini-N-WASP as a function of both Cdc42 and PIP₂ concentration (Fig. 4B). High concentrations of either input alone (~3 μM Cdc42 or ~8 μM PIP₂) are required to yield 50% activation. However, costimulation with 10-fold less of each input yields the same degree of activation. The observed behavior closely fits that predicted by our model with a cooperativity factor of >100 linking Cdc42 and PIP₂ activation (20).

These results indicate that N-WASP can exist in a primed state that, although repressed, is preloaded with Arp2/3 and ready for immediate actin filament assembly upon activation (21). The high cooperativity by which this state of N-WASP is activated allows it to detect and amplify weak but coincident signals of both Cdc42 and PIP₂ (Fig. 4C) (22). Thus, N-WASP approximates a coincidence detector or a logical "AND" gate, devices whose output is dependent on stimulation by the proper combination of inputs (23). The mechanism of N-WASP regulation reveals general principles by which simple protein interaction modules, if combined in the proper

cooperative fashion, can yield a sophisticated signal-integrating machine.

Note added in proof: Rohatgi *et al.* (34) have recently also identified the basic motif of N-WASP as the PIP₂ responsive element.

References and Notes

1. C. A. Parent, P. N. Devreotes, *Science* **284**, 765 (1999).
2. T. J. Mitchison, L. P. Cramer, *Cell* **84**, 371 (1996).
3. M. F. Carlier, A. Ducruix, D. Pantaloni, *Chem. Biol.* **6**, R235 (1999).
4. R. D. Mullins, *Curr. Opin. Cell Biol.* **12**, 91 (2000).
5. R. Rohatgi *et al.*, *Cell* **97**, 221 (1999).
6. L. M. Machesky, R. H. Insall, *Curr. Biol.* **8**, 1347 (1998).
7. M. P. Czech, *Cell* **100**, 603 (2000).
8. A. Hall, *Science* **279**, 509 (1998).
9. A. S. Kim, L. T. Kakalis, N. Abdul-Manan, G. A. Liu, M. K. Rosen, *Nature* **404**, 151 (2000).
10. H. Miki, T. Sasaki, Y. Takai, T. Takenawa, *Nature* **391**, 93 (1998).
11. The specific sequence of the basic motif [NISHT-KEKKKGAKKKRLTK (24)] is essential for repression; mutation of nine lysines to alanine abolishes repression (K. E. Prehoda, W. A. Lim, data not shown).
12. The measured affinity for the WASP GBD-VCA interaction is $K_d \approx 1 \mu\text{M}$ (9).
13. K. E. Prehoda, W. A. Lim, data not shown.
14. Like full-length N-WASP, the degree of mini-N-WASP activation is dependent on the nucleotide state of Cdc42 (5). Our findings with mini-N-WASP show that the enabled/VASP homology 1 (EVH1) domain and proline-rich region are unnecessary for this mode of regulation. These other domains may be involved in targeting [V. Moreau *et al.*, *Nature Cell Biol.* **2**, 441 (2000)] or in modes of regulation distinct from that mediated by the control region. Our findings contradict previous suggestions that the EVH1 domain is the input point for PIP₂ activation (5) [H. Miki, K. Miura, T. Takenawa, *EMBO J.* **15**, 5326 (1996); K. E. Prehoda, D. J. Lee, W. A. Lim, *Cell* **97**, 471 (1999)]. We found that the N-WASP EVH1 domain is a peptide-binding module and does not bind acidic phospholipids (K. E. Prehoda, J. A. Scott, W. A. Lim, in preparation).
15. Addition of high concentrations of the control region can apparently inhibit interaction of Arp2/3 with the VCA domain. However, interpretation of this experiment is complicated by our subsequent finding that there is a second Arp2/3-binding site in the control region (see below) which can, at stoichiometric excess, competitively deplete available Arp2/3.
16. D. A. Fruman, L. E. Rameh, L. C. Cantley, *Cell* **97**, 817 (1999).
17. H. Stenmark, R. Aasland, *J. Cell Sci.* **112**, 4175 (1999).
18. J. Monod, J. P. Changeux, F. Jacob, *J. Mol. Biol.* **6**, 306 (1963).
19. M. F. Perutz, *Sci. Am.* **239**, 92 (December 1978).
20. This value is likely to be a lower estimate for the cooperativity *in vivo*, since activated Cdc42 is normally prenylated [F. L. Zhang, P. J. Casey, *Annu. Rev. Biochem.* **65**, 241 (1996)]. Thus, both inputs would be restricted to the membrane, and their effective concentrations with respect to one another would be even higher.
21. These results show that exclusion of Arp2/3 is not required for repression. However, it is possible that other elements in full-length N-WASP function by blocking Arp2/3 binding.
22. This model predicts that N-WASP will have a limited range of optimal sensitivity. High concentrations of either individual input can overload the system, consistent with observations that either overexpression of a Cdc42 exchange factor [Y. Zheng *et al.*, *J. Biol. Chem.* **271**, 33169 (1996)] or phosphoinositide 5-kinase [A. L. Rozelle *et al.*, *Curr. Biol.* **10**, 311 (2000)] results in unregulated actin polymerization. N-WASP's signal integration properties are likely optimized for the physiologically relevant range of input concentrations, just as the oxygen-binding properties of hemoglobin are set for the observed range of oxygen partial pressure [M. Perutz, *Cooperativity and*

Allosteric Regulation in Proteins (Cambridge Univ. Press, Cambridge, 1990)].

23. H. R. Bourne, R. Nicoll, *Cell (Suppl.)* **72**, 65 (1993).
24. Single-letter abbreviations for the amino acid residues are as follows: A, Ala; C, Cys; D, Asp; E, Glu; F, Phe; G, Gly; H, His; I, Ile; K, Lys; L, Leu; M, Met; N, Asn; P, Pro; Q, Gln; R, Arg; S, Ser; T, Thr; V, Val; W, Trp; and Y, Tyr.
25. N-WASP fragments were cloned by polymerase chain reaction from a rat cDNA library. Proteins were expressed as fusions to either a polyhistidine tag or glutathione S-transferase (GST). Proteins were expressed in *Escherichia coli* (BL21-DE3) and purified by chromatography on Ni-NTA resin (Qiagen) or glutathione agarose resin (Sigma), followed by Source 5 or Q resins (Pharmacia). The polyhistidine tag was removed by incubation with tobacco etch virus (TEV) protease, except when required for detection in Western blots.
26. Actin polymerization assays were performed as described [L. M. Machesky *et al.*, *Proc. Natl. Acad. Sci. U.S.A.* **96**, 3739 (1999)]. Briefly, polymerization of actin doped with 1.2% pyrene-labeled actin was monitored via change in fluorescence (excitation: 366 nm; emission: 407 nm). Before the reaction, actin was converted from the Ca-ATP to the Mg-ATP form by adding MgCl₂ and EGTA to final concentrations of 50 and 200 μM, respectively, and incubating at 25°C for 2 min. To initiate polymerization, actin was added to a solution containing Arp2/3 and any other factors at 20°C. Final conditions were 2.5 μM total actin, 50 mM KCl, 1 mM MgCl₂, 1 mM EGTA, 10 mM imidazole (pH 7.0), 0.2 mM ATP, and 1 mM DTT in a volume of 100 μl. Arp2/3 and actin were purified from *Acanthamoeba castellanii* as described in the above reference. Rabbit skeletal muscle actin was pyrene-labeled as described [S. MacLean-Fletcher, T. D. Pollard, *Cell* **20**, 329 (1980)].
27. GST-fusion binding assays were performed by immobilizing GST-fusion proteins on glutathione agarose beads (Sigma). We incubated 5 μl of beads with the appropriate target proteins in binding buffer [20 mM HEPES (pH 7.0), 100 mM NaCl, 1 mM dithiothreitol (DTT)] in a total volume of 100 μl (final GST-fusion concentration of ~10 μM). After gentle rotation at 4°C for 30 min, beads were washed three times with 1 ml binding buffer plus 0.05% Tween-20. Bound proteins were analyzed by SDS-polyacrylamide gel electrophoresis (SDS-PAGE) and visualized by coomassie blue staining or by Western blotting with anti-Arp2 or anti-polyhistidine antibodies (Qiagen).
28. Human Cdc42 was expressed in *E. coli* as a fusion to GST, and activated by incubating with 100 μM GTPγS for 30 min at room temperature, followed by addition of MgCl₂ to a 10 mM final concentration [C. Egile *et al.*, *J. Cell Biol.* **146**, 1319 (1999)]. The GST tag was removed by thrombin cleavage at 4°C for 2 hours, followed by purification on a Source Q column. Vesicles containing phosphatidylinositol 4-phosphate (PIP) or PIP₂ (48:48:4 of dibromo-phosphatidyl choline:phosphatidyl serine: PIP or PIP₂) were prepared by dissolving phospholipids in chloroform, drying under nitrogen, resuspending in 20 mM HEPES (pH 7.0), 100 mM NaCl, and 1 mM DTT, and passing through >10 freeze-thaw/bath sonication cycles. Approximate concentrations of PIP₂ or PIP were calculated by dividing the total concentration by two, since 50% of the total was assumed to be on the inside layer of the vesicles.
29. Cosedimentation lipid vesicle binding assays were performed as described [J. M. Kavan *et al.*, *J. Biol. Chem.* **273**, 30497 (1998)] by mixing 3 μM protein and vesicles (~20 μM PIP or PIP₂) in 20 mM HEPES (pH 7.0), 100 mM NaCl, and 1 mM DTT (total assay volume 65 μl), incubating at 25°C for 10 min, and centrifuging at 100,000g for 1 hour. The vesicle pellet was washed with 200 μl of buffer and suspended in a volume of buffer equal to the supernatant. Bound (pellet) and unbound proteins (supernatant) were identified by SDS-PAGE.
30. Supplemental figures are available at www.sciencemag.org/feature/data/1054208.shl
31. Although we found that repressed mini-N-WASP

still interacts with Arp2/3, we do not know whether Arp2/3 binds to a composite site including elements from both the VCA and B-GBD fragments (as modeled in Fig. 2D), or if it only interacts with the B-GBD site. We only know that the second binding site helps shift the VCA-Arp2/3 complex into a nonproductive conformation.

32. M. G. Rudolph *et al.*, *J. Biol. Chem.* **273**, 18067 (1998).

33. Simulation of cooperativity model. The fractional activity of N-WASP was calculated to be

$$\theta = \frac{K_B[A] + K_A[B] + c[A][B]}{K_A K_B + K_B[A] + K_A[B] + c[A][B]}$$

where [W] is the concentration of mini-N-WASP, [A] is the total concentration of input molecule A, [B] is the total concentration of input molecule B, c is the cooperativity factor linking binding of A and B, and

$$K_A = \frac{[W][A]}{[W \cdot A]} \quad K_B = \frac{[W][B]}{[W \cdot B]}$$

$$\frac{K_A}{c} = \frac{[W \cdot B][A]}{[W \cdot A \cdot B]} \quad \frac{K_B}{c} = \frac{[W \cdot A][B]}{[W \cdot A \cdot B]}$$

This model assumes that $[W_{\text{tot}}] \ll [A]$ and $[B]$, and that species WA, WB, and WAB have equal activity (W is inactive). Theoretical curves describing the behavior for different values of c were calculated

using the program Mathematica (Wolfram Research, www.wolfram.com).

34. R. Rohatgi, H. H. Ho, M. W. Kirschner, *J. Cell Biol.* **150**, 1299 (2000).

35. We thank J. Zalevsky for reagents and helpful discussions and H. Bourne, V. Denic, D. Julius, B. Kelch, H. Madhani, J. Weissman, and members of the Lim lab for comments and discussion. Supported by grants to W.A.L. from NIH, the Burroughs Wellcome Young Investigator Program, the Searle Scholars Program, and the Packard Foundation. K.E.P. is a Cancer Research Institute Postdoctoral Fellow.

20 July 2000; accepted 18 September 2000

Direct Coupling Between Meiotic DNA Replication and Recombination Initiation

Valérie Borde,¹ Alastair S. H. Goldman,² Michael Lichten^{1*}

During meiosis in *Saccharomyces cerevisiae*, DNA replication occurs 1.5 to 2 hours before recombination initiates by DNA double-strand break formation. We show that replication and recombination initiation are directly linked. Blocking meiotic replication prevented double-strand break formation in a replication-checkpoint-independent manner, and delaying replication of a chromosome segment specifically delayed break formation in that segment. Consequently, the time between replication and break formation was held constant in all regions. We suggest that double-strand break formation occurs as part of a process initiated by DNA replication, which thus determines when meiotic recombination initiates on a regional rather than a cell-wide basis.

During meiosis in most organisms, division of the diploid genome among haploid gametes is accompanied by frequent recombination between homologous parental chromosomes. Recombination occurs after meiotic DNA replication but before the first meiotic division. In the yeast *Saccharomyces cerevisiae*, blocking meiotic replication has been shown to prevent recombination (1–4), but the connection between these two fundamental processes remains unknown. A replication dependence of meiotic recombination would be expected if replication-inhibited cells could not form the double-strand breaks (DSBs) that initiate recombination. This could result either from a direct coupling between replication and DSBs or from checkpoint systems that sense incomplete replication and prevent DSB formation.

To test these suggestions, we examined DSBs in cells undergoing meiosis in the presence of 100 mM hydroxyurea (HU), a concentration that prevents DNA replication (4). In such conditions, meiotic progression is

normally blocked before the first nuclear division (meiosis I) by the *MEC1*-dependent checkpoint system; progression is restored in *mec1-1* mutants (4). Wild-type cells sporulated in HU did not form DSBs, and meiotic progression was blocked (5). By contrast, about 40% of *mec1-1* mutant cells progressed through the meiosis I in the presence of HU, but DSBs still did not form (Fig. 1). Thus, the failure to form DSBs without replication is not due to a *MEC1*-dependent checkpoint block to meiotic progression, making it likely that replication is directly required for DSB formation. This conclusion is reinforced by the finding that *clb5 clb6* double mutants, which prevent meiotic replication without inducing the *MEC1* block (4), also fail to form DSBs (6).

To further examine the relation between replication and DSBs, we used two methods to delay replication in the left arm of chromosome III (*chrIII-L*). One approach used an *ars305 ars306 ars307* triple mutation to inactivate all meiotic replication origins on *chrIII-L* (7) (Fig. 2A). The *ars305 ars306 ars307 chrIII-L* is replicated passively by forks initiating at *ARS309* on the right arm (*chrIII-R*) or further to the right, at least 126 kb from the left-hand telomere. On the basis of a fork progression rate of 2 kb/min (8), replication of the *ars305 ars306 ars307 chrIII-L* should take at least 40 min longer

than when these origins are present and active. The other approach used a reciprocal translocation (*his4::TEL1-L*, Fig. 2A), replacing the first 70 kb of chromosome III with the first 4 kb of chromosome I (*TEL1-L*). This places *TEL1-L* next to the *HIS4-CEN3* region, which undergoes frequent DSBs (9) and contains the early-firing origin *ARS306* (10). Yeast telomeres are late replicating and impose this property on nearby sequences (11, 12), so this translocation should delay replication in the *HIS4-CEN3* region.

We monitored meiotic replication on chromosome III by two-dimensional (2D) gel electrophoresis of replication intermediates (13). Replication occurred simultaneously at three locations on the normal chromosome III (Fig. 2D). By contrast, in *ars305 ars306 ars307* strains, replication on *chrIII-L* was delayed by 60 min relative to *chrIII-R* (Fig. 2, B and D), as expected if *chrIII-L* was replicated passively by forks initiating on *chrIII-R*. On *his4::TEL1-L*, replication in the *HIS4-CEN3* region was delayed by 30 min relative to *chrIII-R* (Fig. 2D), and most *ARS306* origin activity was eliminated (5), as expected for a telomere position effect on replication.

Delaying replication did not markedly affect DSB frequencies on *chrIII-L*, as measured from blots of pulsed-field gels (Fig. 2C). Maximum DSB levels on the *ars305 ars306 ars307 chrIII-L* were identical to those on the normal chromosome (20% ± 6% compared with 20% ± 5%), as were break levels at individual sites (5). DSBs between *HIS4* and *CEN3* on *his4::TEL1-L* were modestly reduced (6 ± 2% compared with 12 ± 2% on a normal chromosome), the reduction being stronger near *TEL1* than near *CEN3*. However, delaying replication locally had a distinct, reproducible effect on DSB timing (Fig. 2, C and D). DSBs formed simultaneously (1.5 to 2 hours after replication) in both arms of the normal chromosome III. By contrast, overall DSB formation in the late-replicating *ars305 ars306 ars307 chrIII-L* was delayed by 30 min compared with *chrIII-R* (Fig. 2, C and D). Thus, the time interval between replication and DSB formation was maintained in both arms. Furthermore, the DSB delay in the originless *chrIII-L* varied with distance from active right-arm

¹Laboratory of Biochemistry, Division of Basic Science, National Cancer Institute, Bethesda, MD 20892–4255, USA. ²Department of Molecular Biology and Biotechnology, University of Sheffield, Sheffield S10 2TN, UK.

*To whom correspondence should be addressed. E-mail: lichten@helix.nih.gov